Highly Efficient Photoelectron Emission from Stable Low-Work-Function Surfaces Using Organic Bases

Manato Tateno[1], Miyu Moriyama[1], Masahiro Ohara[2], Katsuyuki Morii[3,4,5], Munehiro Hasegawa[3], Hisao Ishii[1,5,6], Hirohiko Fukagawa[1,5,6]

[1]Graduate School of Science and Engineering, Chiba University, 1-33 Yayoi-cho, Inage-ku, Chiba 263-8522, Japan
[2]Faculty of Engineering, Shinshu University, 4-17-1, Wakasato, Nagano 380-8553, Japan
[3]Nippon Shokubai Co., Ltd., 5-8 Nishi Otabi-Cho, Suita, Osaka 564-8512, Japan
[4]Nippon Shokubai Research Alliance Laboratories, Osaka University, 2-1 Yamadaoka, Suita, Osaka 565-0871, Japan
[5]Center for Frontier Science, Chiba University, 1-33 Yayoi-cho, Inage-ku, Chiba 263-8522, Japan
[6]Molecular Chirality Research Center, Chiba University, 1-33 Yayoi-cho, Inage-ku, Chiba 263-8522, Japan

ABSTRACT

Photocathodes based on alkali metals such as cesium (Cs) exhibit high quantum efficiency (QE) owing to their low work functions (WFs). However, their poor stability and short lifetimes under vacuum conditions limit their practical application. In this study, we demonstrate that modifying electrodes with phenanthroline derivatives achieves ultra-low WFs of 2.2 eV while significantly enhancing stability compared to Cs under both high vacuum (~10^{-5} Pa) and ultra-high vacuum (~10^{-8} Pa) conditions. Notably, 4,7-bis(1-pyrrolidinyl)-1,10-phenanthroline exhibited greater stability than Cs and achieved more than twice the QE of Cs in the 2.7–3.5 eV photon energy range, without relying on negative electron affinity structures. These findings demonstrate the potential of organic low-WF materials as alternatives to alkali metals for photocathode applications, offering extended photoemission lifetimes under less stringent vacuum conditions.

Photocathodes serve as fundamental components in various applications, such as the first cathode of a photomultiplier tube, electron source for radio-frequency electron guns, and equipment in synchrotron radiation facilities [1–3]. Photocathodes are broadly classified into metal photocathodes (e.g., copper, magnesium, and alkali metals) and semiconductor photocathodes (e.g., cesium telluride and gallium arsenide (GaAs)).[4] Material choices are guided by factors such as their quantum efficiency (QE) as a function of light wavelength, operational lifetime, response speed, and required cathode current.

High photoelectron emission efficiency is required for photocathodes; thus, materials with low work functions (WF), such as alkali metals, are widely used. However, achieving both low WF and high stability remains a significant challenge. Cesium (Cs), one of the lowest known WFs (~2 eV), has been extensively studied for photocathode applications.[5–7] In particular, negative electron affinity (NEA) structures based on GaAs surfaces modified with Cs, which exhibit high QE in the visible light region, have been the subject of intensive research in recent years.[4,8–10]

However, Cs-based photocathodes have serious problems, such as being usable only in ultrahigh vacuum (UHV) and extremely limited operational lifetimes. These limitations are due to the high chemical reactivity of Cs surfaces, which readily increases its WF when exposed to residual gases such as oxygen, moisture, and carbon dioxide. [11] To suppress this reactivity, an extremely high vacuum of approximately 10^{-9} Pa is required; however, studies on NEA GaAs photocathodes show that even under such stringent conditions, their QE can halve in approximately 1 h.[12] In other words, although a low-WF surface is suitable for a photocathode, stability, and low WF are in a tradeoff relationship, and achieving both is challenging. To address these problems, various research efforts have been conducted recently to extend the lifetime of photocathodes. One method involves the use of p-doped gallium nitride (GaN), whose wider bandgap allows for a stable NEA surface, providing four times the lifetime of GaAs [12–14]. The other involves developing Cs-free GaN photocathodes with a stepwise controlled doping concentration to achieve both 10% QE and high stability.[15] Although these efforts have achieved some success in extending the lifetime of NEA photocathodes, stable long-term performance remains difficult even in extremely high vacuum. Therefore, advancing photocathode technology necessitates the development of low-WF surfaces that combine high photoelectron emission efficiency with robust stability.

Low-WF materials are crucial not only in photocathodes but also in various devices such as light-emitting diodes and solar cells made of organics, perovskites, and quantum dots.[16–19] In recent years, low-WF materials using oxides, polymers, and organic molecules have been developed.[16,17,19–22] For instance, zirconium oxide, which is widely used as a Schottky emitter material exhibits a WF of 2.7 eV [23]. Polyethyleneimine (PEI) is a polymer that is widely used as a cathode material in organic light-emitting diodes (OLEDs) and organic photovoltaics.[16] The WF was 3.1 eV when formed on a zinc oxide (ZnO) surface. In contrast, the WF of aluminum (Al) and ZnO surfaces (~ 4 eV) can be controlled in the range of approximately 3–2 eV using phenanthroline (Phen) derivatives and strong organic bases.[20–22,24] This is because the coordination reaction at the metal–organic interface can generate a substantial WF change of more than 2 eV. These low WF electrodes modified with organic materials exhibit high electron injection properties, and OLEDs using these electrodes emit light at extremely low applied voltages. Furthermore, dark spot formation on the emissive surface is significantly suppressed compared to alkali-metal-based OLEDs, leading to enhanced operational stability even in environments where oxygen and moisture can penetrate. Generally, organic molecules contribute to surface stability because they lack dangling bonds, making them less prone to oxidation. Therefore, low-WF electrodes modified with these organic materials are more stable against residual gases in vacuum than alkali-metal electrodes, potentially leading to dramatically improved photocathode lifetimes. However, reports on the stability of organic low-WF surfaces and their actual photoemission efficiency under light irradiation, which is crucial for photocathode applications, are currently unavailable.

In this study, we demonstrated that electrodes modified with Phen derivatives achieve WFs ranging from 3.0 to 2.2 eV and exhibit remarkable stability and photoelectron emission efficiency. The stability and photoemission properties of the Phen-modified electrodes were compared with those of Cs. Under high-vacuum (HV, ~10^{-5} Pa) conditions, the WF of Cs increased by approximately 0.4 eV over 100 min, whereas the increase for all the Phen-modified electrodes was less than 0.1 eV. The QE of 4,7-bis(1-Pyrrolidinyl)-1,10-phenanthroline (p-Pyrrd-Phen)–modified electrode was more than twice that of Cs in the 2.7–3.5 eV photon energy range. The photoelectron energy distribution of p-Pyrrd-Phen, which showed the highest QE, revealed that high QE could be achieved without relying on NEA structures. The identification of low-WF organic materials suitable for photocathode applications is a significant advancement, expanding surface modification possibilities and offering a promising path toward more stable, longer-lifetime photocathodes operable under low vacuum conditions.

The Phen derivatives: p-Pyrrd-Phen, 4,7-diphenyl1,10-phenanthroline (BPhen), and 2,9-Dimethyl-4,7-diphenyl-1,10-phenanthroline (bathocuproine, BCP) (Fig. 1(a)), were provided by Nippon Shokubai Co., Ltd. These materials were deposited onto a 1.0-nm-thick layer of Al (NILACO: purity 99.99 %) or silver (Ag, NILACO: purity 99.99 %) that had been deposited on an indium tin oxide (ITO) substrate to a thickness of 3.0 nm. Low-WF surfaces can be produced using the coordination reaction between the Phen derivatives and metals. Several metal substrates, including ITO, were prepared, and Phen derivatives were deposited on each substrate to verify that the coordination strength depends on the metal species. An alkaline dispenser (SAES Getters S.p. A: CS/NF/3.9/12 FT10+10) was used to directly deposit Cs onto an ITO substrate. Isopropanol, acetone, and a UV ozone cleaner (SEN LIGHT Corporation: SSP16-110) were used to clean the ITO substrates. The deposition rates of the Phen derivatives were approximately 1.0 Å/s, more than 2.0 Å/s for Al, and 0.3 Å/s for Cs. During vacuum deposition, WF measurements were performed using a homemade Rotary Kelvin Probe (RKP) under HV conditions.[25] The WF of the reference electrode made of stainless steel (SUS304, mainly iron, chromium ~18%, nickel ~8%) was 4.43 eV. When measured by RKP, the working pressure was maintained between 7×10^{-5} and 1×10^{-4} Pa. A Tektronix KEITHLEY 6430 sub-femtoampere source measuring unit and photomultiplier tubes (Hamamatsu Photonics: R376, R6836) were used to conduct QE measurements in the reflection mode. The photon flux was calculated by considering the viewport transmittance, gain, and spectral sensitivity of the photomultiplier tubes. A deuterium lamp (Hamamatsu Photonics: L1835, 150 W) and a xenon lamp (Ushio: UXL-500D, 500

W) were used as light sources, and the emitted light was monochromatized using a zero-dispersion double monochromator (Bunkoukeiki: BIP-M25-GTM). Ultraviolet photoelectron spectroscopy (UPS) was performed by irradiating a sample with light with a photon energy of 7.7 eV. Electrons emitted perpendicularly from the sample surface were collected using an electrostatic hemispherical analyzer (PSP: RESOLVE120). After depositing the sample in a deposition chamber maintained at 8×10^{-6} Pa, the photoelectron emission properties were determined in a measuring chamber maintained at 6×10^{-8} Pa and applying -10 V on the sample. Further details on the experimental setup have been described in previous studies.[25,26]

Figure 1(b) shows the RKP measurement results of the WF during the deposition of the Cs and Phen derivatives under HV conditions. During Cs deposition, the WF time-dependent variation and instability were observed by measuring it with RKP during film growth. Figure 1(b) shows an unstable decrease in WF upon Cs deposition on ITO (blue line). The WF reached 2.29 eV, which was immediately increased. In contrast, the WFs of the Phen derivatives vacuum-deposited on Al-coated ITO, BCP (green line), BPhen (blue line), and p-Pyrrd-Phen (red line) decreased immediately to 3.08, 2.80, and 2.27 eV, respectively, and thereafter remained highly stable. A similar trend was observed for p-Pyrrd-Phen deposited directly on ITO (violet line) and Ag-coated ITO (black line), resulting in WFs of 3.93 and 2.37 eV, respectively. Among the substrates tested, Al exhibited the lowest WF. This could be due to different interactions between the metals and the p-Pyrrd-Phen, which arise from variations in the atomic radii and outer-shell orbitals of the surface metal atoms. The instability observed during the deposition of Cs (Fig. 1(b)) is attributed to the chemical reactions and the physical adsorption of residual gases such as water.[27] In addition, alternating surface contamination and film formation may occur because pure Cs have low cohesive energy and does not form multilayers at room temperature [28]. As a result, the WF of Cs in Fig. 1(b) fluctuated and reached its minimum value even during deposition. Therefore, the low WF surface formation process for Phen derivatives is more stable and reproducible than that of Cs.

Figure 2(a)–(c) shows the stabilities of WF after deposition under HV and UHV conditions. Under HV conditions, the WF shift from the end of deposition (ΔWF) for Cs (blue line) fluctuated and increased by up to 0.4 eV after 100 min (Fig. 2(a)). In contrast, the Phen derivatives remained highly stable, with an increase of less than 0.1 eV. A different experimental setup than that used for Fig. 2(a) was used to conduct stability evaluations under UHV conditions (Figs. 2(b) and (c)). The WFs of Cs (blue line), BCP (green line), BPhen (orange line), and p-Pyrrd-Phen (red line) were 2.15, 3.03, 2.89, and 2.18 eV, respectively, immediately after deposition under UHV conditions (Fig. 2(b)). After 1000 min, the WF of Cs increased by more than 0.1 eV, whereas that of Phen derivatives increased by less than 0.05 eV (Fig. 2(c)). As a metal, Cs is highly reactive because of its low WF and ionization potential (IP). In contrast, organic molecules generally exhibit large band gaps and, despite having low WFs, have relatively high IPs, resulting in lower chemical reactivity. The Phen derivatives do not have electron-donating capabilities similar to those of Cs because their IPs are approximately 5 eV. Both the formation of an interface dipole and chemical bonding between the substrate and molecules are responsible for the reduction in WF induced by the Phen derivatives.[21] This difference in the mechanism of WF reduction is the reason for the excellent WF stability of the Phen derivatives (Figs. 2(a)–(c)). Thus, an electrode modified with p-Pyrrd-Phen and Al offers significantly higher stability under both HV and UHV conditions, while displaying a WF as low as that of Cs.

Figure 3(a) shows the QE measurement results under UHV conditions. The vertical axis represents logarithmic QE, and the horizontal axis corresponds to the incident photon energy. The QEs of p-Pyrrd-Phen (red line), BPhen (orange line), BCP (green line), and Cs (blue line) (Fig. 3(a)), were measured by photocurrent detection using a source measuring unit. In contrast, the QE curve of ITO (black line) was determined by normalizing its photoelectron yield spectrum, which was measured with high sensitivity using a photomultiplier tube that was calibrated using the QE value of the photon energy of 7.7 eV that was obtained by photocurrent measurement. The QE of ITO at other photon energies was too low to be measured using the source measuring unit; hence, this method was required. A correlation between WF (Fig. 2(b)) and QE emission threshold values (Fig. 3(a)) was observed when comparing the Phen derivatives. Furthermore, high QEs were obtained for Cs and the Phen derivatives in all photon energy ranges above their respective WFs. This indicates that a low WF is essential for high QE. As shown in Fig. 3(a), the QE of Cs decreased relative to that of p-Pyrrd-Phen at photon energies above 5.4 eV, most likely because of an increase in the WF during the measurement. During the QE measurements, the WF of Cs increased by 0.04 eV. Although the WFs of p-Pyrrd-Phen and Cs in Fig. 2(b) were similar, the QE of p-Pyrrd-Phen was more than twice that of Cs in the photon energy range of 2.7–3.5 eV. Above 3.5 eV, the QE of Cs increased, approaching that of p-Pyrrd-Phen. To further investigate the QE characteristics, the density of states (DOS) was determined using UPS; the results are shown in Fig. 3(b). The horizontal axis represents the binding energy relative to the vacuum level. According to previous studies, the underlying Al and in-gap states formed between the molecules and substrate originate from the shallow-energy structure observed near the Fermi level in Phen derivatives.[21,29–32] In addition, the relative intensity of the DOS of Cs and p-Pyrrd-Phen reversed at a binding energy of 3.3 eV, indicating that p-Pyrrd-Phen has a shallower energy structure than Cs. The QE differences between p-Pyrrd-Phen and Cs are probably due to variations in DOS. Furthermore, differences in the optical reflectivity and photoionization cross-section may contribute to the higher QE of p-Pyrrd-Phen. Generally, metals with free electrons exhibit higher reflectivity than organic molecules with localized electrons. Moreover, the outer-shell electron of Cs is in the 6s orbital, which has a relatively lower photoionization cross-section (0.1–0.2 Mb) under low-energy photon excitation.[33] In Fig. 3(a), a shoulder-like structure is observed at approximately 3.8 eV in all the spectra. The photon energy itself, rather than the DOS, is responsible for this increase in QE because the UPS data shown in Fig. 3(b) does not contain any similar feature. Previous studies have shown that ITO exhibits an absorption onset at 3.2 eV, which aligns well with the observed QE features.[34] This implies that photon absorption in the ITO substrate could be due to the increase in QE. Overall, these results demonstrate that p-Pyrrd-Phen exhibits superior QE characteristics compared to Cs because of the combination of its WF and DOS.

To further investigate the superior photoemission properties of p-Pyrrd-Phen, photoelectron emission spectroscopy was used with various photon energies. Figures 4(a)–(c) show the photoelectron emission spectra obtained at incident photon energies ranging from 2.4 eV to 5.0 eV. The vertical axis represents the photoelectron intensity normalized to the incident photon flux, and the horizontal axis corresponds to the kinetic energy of the emitted electrons. The spectral width increased proportionally with photon energy. This relationship is not straightforward in NEA photocathodes such as GaAs because electrons are tunneled through the surface potential barrier.[35,36] This indicates that photoemission from p-Pyrrd-Phen follows the conventional three-step model rather than NEA. Notably, even in the absence of NEA, such high photoemission efficiency can be achieved (Fig. 3(a)). A secondary electron peak begins to emerge at an incident photon energy of 3.4 eV and increases significantly with higher photon energies, according to the shape of each spectrum (Figs. 4(a)–(c)). The threshold energy of 3.4 eV is consistent with the onset of the structure commonly observed in all the spectra shown in Fig. 3(a). Furthermore, the spectrum obtained using an ITO substrate exhibited a more intense secondary electron peak than that obtained using highly oriented pyrolytic graphite (HOPG), according to a comparison of UPS spectra for BPhen on Al with HOPG substrates (Supplementary Fig. 1). These results demonstrate that the photoelectrons generated within the ITO substrate are emitted as secondary electrons into the vacuum. This indicates that selecting an appropriate substrate that facilitates a strong internal photoelectric effect can enhance the QE even when designing a photocathode using p-Pyrrd-Phen.

In conclusion, we demonstrated that the Phen derivatives can form stable low-WF surfaces with excellent photoelectron emission properties, making them highly promising materials for photocathode surface modification. The WFs of p-Pyrrd-Phen and BPhen exhibit lower WFs than Cs and are more stable under HV conditions. In addition, even under UHV, p-Pyrrd-Phen maintained a lower WF than Cs and a QE that was more than twice as high as Cs in the 2.7–3.5 eV photon energy range. Furthermore, high QE was achieved without the use of NEA structures. The identification of this low-WF organic material is a significant advancement, expanding the range of viable photocathode surface modification materials to include organic molecules. The proposed design also introduces the potential for long-lifetime photocathodes to be operable in lower vacuum conditions. Future studies should combine Phen derivatives with substrates exhibiting strong internal photoelectric effect efficiency and GaAs or GaN, which can also form NEA surfaces.

SUPPLEMENTARY MATERIAL

See the supplementary material for UPS spectra measured using photon energy light for BPhen deposited on Al with different substrates: ITO and HOPG.

ACKNOWLEDGMENTS

This research was financially supported by the Japan Society for the Promotion of Science (JSPS) KAKENHI Grant-in-Aid for Scientific Research (Grant No. 24K23071).

AUTHOR DECLARATIONS

Conflict of Interest

The authors have no conflicts to disclose.

Author Contributions

Manato Tateno: Conceptualization (equal); Data curation (lead); Formal analysis (lead); Investigation (lead); Validation (lead); Visualization (lead); Writing – original draft (lead); Writing – review & editing (equal). **Miyu Moriyama:** Data curation (lead); Investigation (lead). **Masahiro Ohara:** Data curation (equal); Formal analysis (equal); Methodology (lead); Resources (lead); Software (lead); Writing – review & editing (equal). **Katsuyuki Morii:** Conceptualization (lead); Resources (lead); Writing – review & editing (equal). **Munehiro Hasegawa:** Conceptualization (equal); Resources (lead). **Hisao Ishii:** Conceptualization (lead); Funding acquisition (lead); Project administration (lead); Resources (lead); Supervision (lead); Validation (lead); Writing – review & editing (lead). **Hirohiko Fukagawa:** Conceptualization (lead); Funding acquisition (lead); Project administration (lead); Resources (lead); Supervision (lead); Validation (lead); Writing – review & editing (lead).

DATA AVAILABILITY

The data that support the findings of this study are available from the corresponding author upon reasonable request.

REFERENCES

[1] R. Foord, R. Jones, C.J. Oliver, and E.R. Pike, "The Use of Photomultiplier Tubes for Photon Counting," Appl. Opt. **8**(10), 1975–1989 (1969).

[2] J. Yang, "Femtosecond Electron Diffraction Using Relativistic Electron Pulses," in *Nov. Imaging Spectrosc.*, (IntechOpen, 2019).

[3] O. Tanaka, N. Higashi, and T. Miyajima, "Injector Optimization for the IR-FEL Operation at the Compact ERL at KEK," Proc. 12th Int. Part. Accel. Conf. **IPAC2021**, 4 pages, 0.655 MB (2021).

[4] J. Schaber, R. Xiang, and N. Gaponik, "Review of photocathodes for electron beam sources in particle accelerators," J. Mater. Chem. C **11**(9), 3162–3179 (2023).

[5] B. Woratschek, W. Sesselman, J. Küppers, G. Ertl, and H. Haberland, "Electron spectroscopy of alkali metal surfaces by deexcitation of metastable He atoms," Surf. Sci. **180**(1), 187–202 (1987).

[6] Triloki, R. Rai, N. Gupta, N.F.A. Jammal, and B.K. Singh, "Photoemission and optical constant measurements of a Cesium Iodide thin film photocathode," Nucl. Instrum. Methods Phys. Res. Sect. Accel. Spectrometers Detect. Assoc. Equip. **787**, 161–165 (2015).

[7] M. Gaowei, J. Sinsheimer, D. Strom, J. Xie, J. Cen, J. Walsh, E. Muller, and J. Smedley, "Codeposition of ultrasmooth and high quantum efficiency cesium telluride photocathodes," Phys. Rev. Accel. Beams **22**(7), 073401 (2019).

[8] J. Scheer, and J. Van Laar, "GaAs-Cs: A new type of photoemitter," Solid State Commun. **3**(8), 189–193 (1965).

[9] A. Turnbull, and G. Evans, "Photoemission from GaAs-Cs-O," J. Phys. Appl. Phys. **1**(2), 155 (1968).

[10] T. Nishitani, M. Tabuchi, Y. Takeda, Y. Suzuki, K. Motoki, and T. Meguro, "High-Brightness Spin-Polarized Electron Source Using Semiconductor Photocathodes," Jpn. J. Appl. Phys. **48**(6S), 06FF02 (2009).

[11] N. Chanlek, J.D. Herbert, R.M. Jones, L.B. Jones, K.J. Middleman, and B.L. Militsyn, "The degradation of quantum efficiency in negative electron affinity GaAs photocathodes under gas exposure," J. Phys. Appl. Phys. **47**(5), 055110 (2014).

[12] T. Nishitani, M. Tabuchi, H. Amano, T. Maekawa, M. Kuwahara, and T. Meguro, "Photoemission lifetime of a negative electron affinity gallium nitride photocathode," J. Vac. Sci. Technol. B **32**(6), 06F901 (2014).

[13] F. Machuca, Z. Liu, Y. Sun, P. Pianetta, W.E. Spicer, and R.F.W. Pease, "Role of oxygen in semiconductor negative electron affinity photocathodes," J. Vac. Sci. Technol. B Microelectron. Nanometer Struct. Process. Meas. Phenom. **20**(6), 2721–2725 (2002).

[14] X. Wang, M. Wang, Y. Liao, L. Yang, Q. Ban, X. Zhang, Z. Wang, and S. Zhang, "Negative electron affinity of the GaN photocathode: a review on the basic theory, structure design, fabrication, and performance characterization.," J. Mater. Chem. C **9**(38), 13013–13040 (2021).

[15] E. Rocco, J. Marini, K. Hogan, V. Meyers, B. McEwen, L.D. Bell, and F. Shahedipour-Sandvik, "Overview and Progress Toward High-Efficiency, Air Stable, Cs-Free III-Nitride Photocathode Detectors," IEEE Photonics J. **14**(2), 1–12 (2022).

[16] Y. Zhou, C. Fuentes-Hernandez, J. Shim, J. Meyer, A.J. Giordano, H. Li, P. Winget, T. Papadopoulos, H. Cheun, J. Kim, M. Fenoll, A. Dindar, W. Haske, E. Najafabadi, T.M. Khan, H. Sojoudi, S. Barlow, S. Graham, J.-L. Brédas, S.R. Marder, A. Kahn, and B. Kippelen, "A Universal Method to Produce Low–Work Function Electrodes for Organic Electronics," Science **336**(6079), 327–332 (2012).

[17] V. Giorgis, F. Morini, T. Zhu, J.-F. Robillard, X. Wallart, J.-L. Codron, and E. Dubois, "Synthesis

and characterization of low work function alkali oxide thin films for unconventional thermionic energy converters," J. Appl. Phys. **120**(20), 205108 (2016).

[18] X. Peng, L. Hu, F. Qin, Y. Zhou, and P.K. Chu, "Low Work Function Surface Modifiers for Solution-Processed Electronics: A Review," Adv. Mater. Interfaces **5**(10), 1701404 (2018).

[19] C.G. Tang, M.N. Syafiqah, Q.-M. Koh, C. Zhao, J. Zaini, Q.-J. Seah, M.J. Cass, M.J. Humphries, I. Grizzi, J.H. Burroughes, R.-Q. Png, L.-L. Chua, and P.K.H. Ho, "Multivalent anions as universal latent electron donors," Nature **573**(7775), 519–525 (2019).

[20] H. Fukagawa, T. Sasaki, T. Tsuzuki, Y. Nakajima, T. Takei, G. Motomura, M. Hasegawa, K. Morii, and T. Shimizu, "Long-Lived Flexible Displays Employing Efficient and Stable Inverted Organic Light-Emitting Diodes," Adv. Mater. **30**(28), 1706768 (2018).

[21] H. Fukagawa, K. Suzuki, H. Ito, K. Inagaki, T. Sasaki, T. Oono, M. Hasegawa, K. Morii, and T. Shimizu, "Understanding coordination reaction for producing stable electrode with various low work functions," Nat. Commun. **11**(1), 3700 (2020).

[22] T. Sasaki, T. Oono, T. Shimizu, and H. Fukagawa, "Effects of Energy-Level Alignment on Operating Voltages of Blue Organic Light-Emitting Diodes," Adv. Mater. Interfaces **10**(19), 2201925 (2023).

[23] H. Satoh, S. Kawata, H. Nakane, and H. Adachi, "Studies on the ZrO/W(100) surface by means of low-energy electron diffraction and X-ray photoelectron spectroscopy," Surf. Sci. **400**(1), 375–382 (1998).

[24] T. Sasaki, M. Hasegawa, K. Inagaki, H. Ito, K. Suzuki, T. Oono, K. Morii, T. Shimizu, and H. Fukagawa, "Unravelling the electron injection/transport mechanism in organic light-emitting diodes," Nat. Commun. **12**(1), 2706 (2021).

[25] M. Ohara, H. Hamada, N. Matsuura, Y. Tanaka, and H. Ishii, "Impact of Intermittent Deposition on Spontaneous Orientation Polarization of Organic Amorphous Films Revealed by Rotary Kelvin Probe," ACS Appl. Mater. Interfaces **15**(49), 57427–57433 (2023).

[26] R. Nakazawa, A. Matsuzaki, K. Shimizu, I. Nakamura, E. Kawashima, S. Makita, K. Tanaka, S. Yasuno, H. Sato, H. Yoshida, M. Abdi-Jalebi, S.D. Stranks, S. Tadano, P. Krüger, Y. Tanaka, H. Tokairin, and H. Ishii, "Reliable measurement of the density of states including occupied in-gap states of an amorphous In–Ga–Zn–O thin film via photoemission spectroscopies: Direct observation of light-induced in-gap states," J. Appl. Phys. **135**(8), 085301 (2024).

[27] M. Kamaratos, E. Giotopoulou, and D. Vlachos, "The interaction mechanism of cesium with water on the SrTiO3(100) surface at room temperature," React. Kinet. Mech. Catal. **135**(6), 3257–3274 (2022).

[28] A.W. Grant, and C.T. Campbell, "Cesium adsorption on TiO2(110)," Phys. Rev. B **55**(3), 1844–1851 (1997).

[29] M.-H. Chen, Y.-H. Chen, C.-T. Lin, G.-R. Lee, C.-I. Wu, D.-S. Leem, J.-J. Kim, and T.-W. Pi, "Electronic and chemical properties of cathode structures using 4,7-diphenyl-1,10-phenanthroline

doped with rubidium carbonate as electron injection layers," J. Appl. Phys. **105**(11), 113714 (2009).

[30] M. Aoki, S. Toyoshima, T. Kamada, M. Sogo, S. Masuda, T. Sakurai, and K. Akimoto, "Level alignment of gap state at organic-metal interface," J. Appl. Phys. **106**(4), 043715 (2009).

[31] T. Sakurai, S. Toyoshima, H. Kitazume, S. Masuda, H. Kato, and K. Akimoto, "Influence of gap states on electrical properties at interface between bathocuproine and various types of metals," J. Appl. Phys. **107**(4), 043707 (2010).

[32] H. Yoshida, "Electron Transport in Bathocuproine Interlayer in Organic Semiconductor Devices," J. Phys. Chem. C **119**(43), 24459–24464 (2015).

[33] H. Sharma, and K. Kumari, "Photoionization cross section of the 6s electron of atomic cesium," Indian J. Phys. B **74B**(1), 89–92 (2000).

[34] N. Biyikli, I. Kimukin, B. Butun, O. Aytur, and E. Ozbay, "ITO-Schottky Photodiodes for High-Performance Detection in the UV–IR Spectrum," IEEE J. Sel. Top. Quantum Electron. **10**(4), 759–765 (2004).

[35] W.E. Spicer, and A. Herrera-Gomez, "Modern theory and applications of photocathodes," edited by K.J. Kaufmann, (San Diego, CA, 1993), p. 18.

[36] L.B. Jones, H.E. Scheibler, S.N. Kosolobov, A.S. Terekhov, B.L. Militsyn, and T.C.Q. Noakes, "Non–monotonic behaviour in the mean transverse energy of electrons emitted from a reflection–mode p-GaAs(Cs,O) photocathode during its QE degradation through oxygen exposure," J. Phys. Appl. Phys. **54**(20), 205301 (2021).

Figures

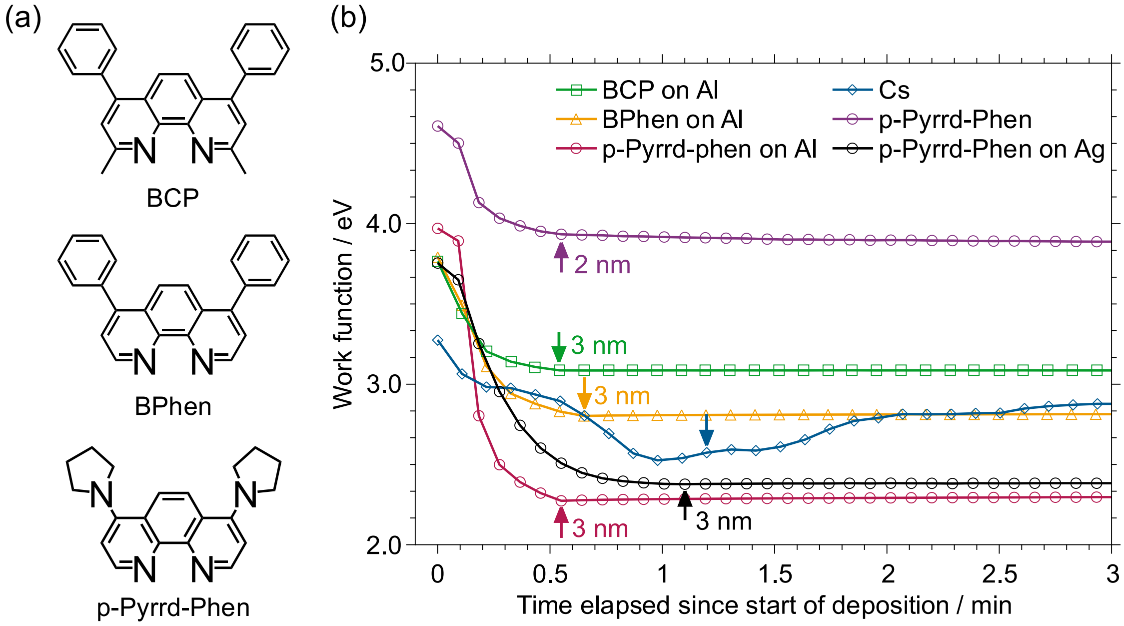

FIG. 1. (a) Molecule structures of phenanthroline (Phen) derivatives (BCP, BPhen, p-Pyrrd-Phen). (b) Work functions during deposition with Phen derivatives and Cs measured using a rotary Kelvin probe under high vacuum conditions. The arrows represent the deposition endpoints.

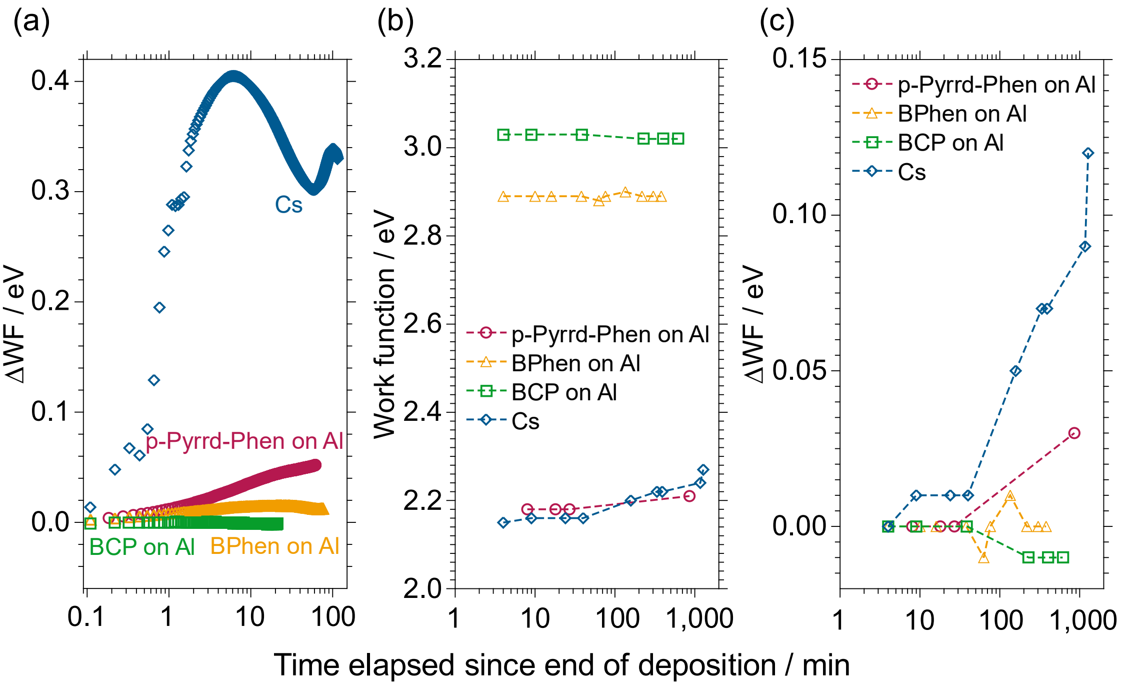

FIG. 2. Stabilities of low work function (WF) surfaces of phenanthroline derivatives (BCP, BPhen, p-Pyrrd-Phen) and Cs. (a) WF shift (ΔWF) relative to the end of deposition under high vacuum conditions. (b) WF, measured using ultraviolet photoelectron spectroscopy under ultra-high vacuum (UHV) conditions. (c) ΔWF under UHV conditions.

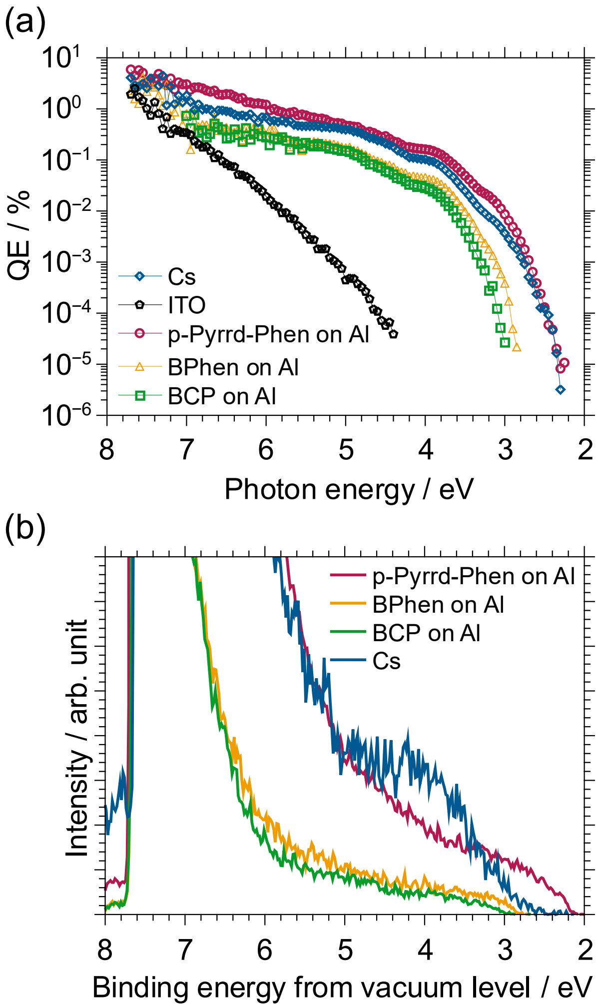

FIG. 3. (a) Quantum efficiency of low work function surfaces with Cs, ITO, and phenanthroline (Phen) derivatives (BCP, BPhen, p-Pyrrd-Phen). (b) Ultraviolet photoelectron spectra of Cs and Phen derivatives, measured using 7.7 eV photon energy.

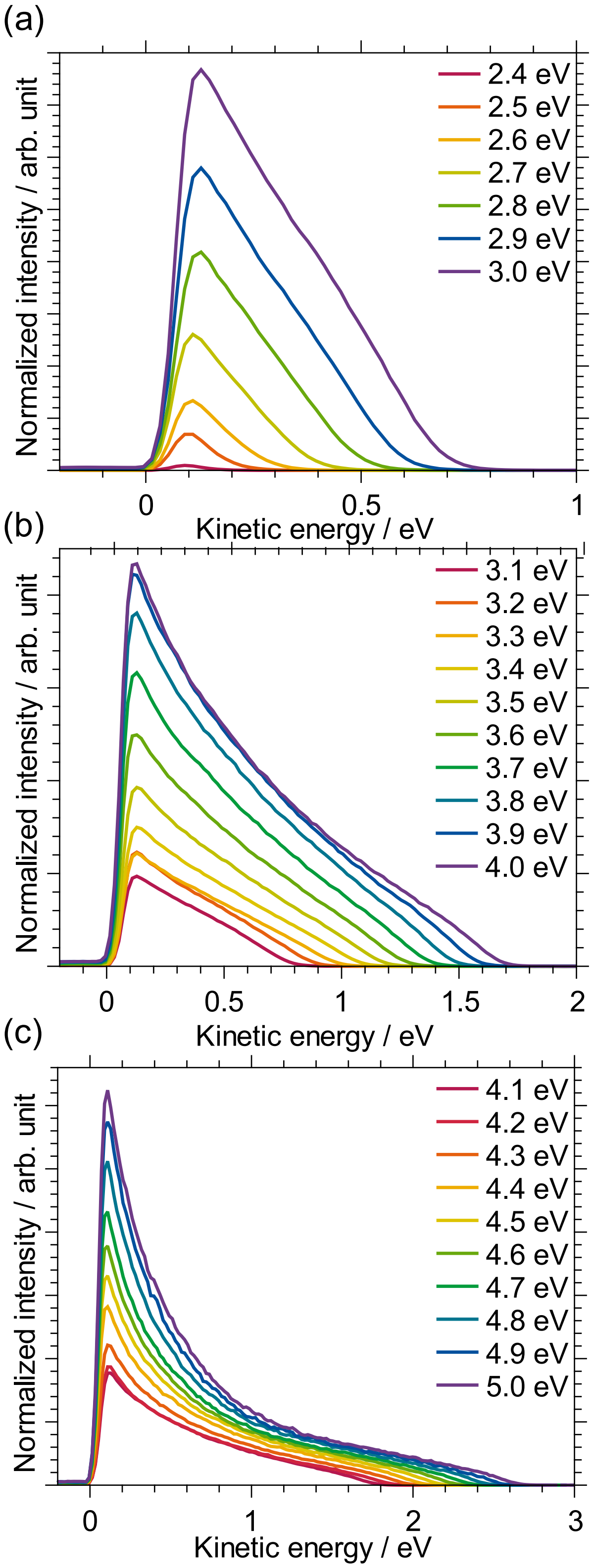

FIG. 4. Photoelectron emission spectra of p-Pyrrd-Phen deposited on Al-coated ITO, measured using photon energies in the ranges of (a) 2.4–3.0, (b) 3.1–4.0, and (c) 4.1–5.0 eV.